This is the peer-reviewed, final accepted version for American Mineralogist, published by the Mineralogical Society of America.
The published version is subject to change. Cite as Authors (Year) Title. American Mineralogist, in press.
DOI: https://doi.org/10.2138/am-2022-8655. http://www.minsocam.org/

Revision 2

S_2^- and S_3^- radicals and the S_4^{2-} polysulfide ion in lazurite, haüyne and synthetic ultramarine blue revealed by resonance Raman spectroscopy

Stefan Farsang[1*], Razvan Caracas[2,3], Takuji B. M. Adachi[4], Cédric Schnyder[5] and Zoltán Zajacz[1]

[1]Department of Earth Sciences, University of Geneva, Rue des Maraîchers 13, 1205 Geneva, Switzerland (*stefan.farsang@unige.ch)

[2]Institut de Physique du Globe de Paris, Université de Paris Cité, CNRS, Paris, France

[3]The Center for Earth Evolution and Dynamics (CEED), University of Oslo, 0371 Oslo, Norway

[4]Department of Physical Chemistry, University of Geneva, Quai Ernest Ansermet 30, 1211 Geneva, Switzerland

[5]Natural History Museum of Geneva, Route de Malagnou 1, 1208 Geneva, Switzerland

Abstract

Taking advantage of the Raman resonance effect, we employed 405 and 532 nm excitations to 1) identify sulfur species present in lazurite, haüyne, and synthetic ultramarine blue pigments and 2) investigate the enigmatic ~485 cm^{-1} band found previously in Raman spectra of lazurite and haüyne collected with 458 nm excitation. In spectra of lazurite and haüyne, bands of the sulfate ion and S_2^- and S_3^- radicals can be seen. Spectra collected using 405 nm excitation show the enhancement of intensity of $\nu_1(S_2^-)$ band and its $n\nu_1$ ($n \leq 7$) progression. Spectra collected using 532 nm incident light show the enhancement of intensity of $\nu_1(S_3^-)$, $\nu_2(S_3^-)$, and $\nu_3(S_3^-)$ bands

and the $n\nu_1$ ($n\leq9$) and $\nu_2 + n\nu_1$ progressions of the $\nu_1(S_3^-)$ band. In spectra collected with 405 nm excitation, we also found features that we ascribe to the S_4^{2-} polysulfide ion. These include the ν_1 symmetric S–S stretching band at ~481 cm^{-1}, the ν_2 symmetric S–S stretching band at ~443 cm^{-1} (only present in spectra of some lazurite samples), the ν_3 symmetric S–S bending at 223 cm^{-1} and the $n\nu_1$ ($n\leq5$) and $n\nu_1+ \nu_3$ progressions of the $\nu_1(S_4^{2-})$ band. We observed that under laser beam, the S_4^{2-} polysulfide ion rapidly decomposes to two S_2^- radicals in lazurite, while it remains stable in haüyne. In spectra of synthetic ultramarine blue pigments, only features of S_2^- and S_3^- radicals were observed. Finally, we verified the identity of the polysulfide ions with *ab initio* molecular dynamics calculations. We conclude that Raman resonance spectroscopy is a powerful qualitative method to detect polysulfide and sulfur radical species with concentrations below the detection limit of conventional analytical techniques. Owing to the high stability of S_4^{2-} in haüyne, this mineral structure appears promising as a host material for S_4^{2-} entrapment, making it potentially useful for applications in optoelectronics.

Keywords

Haüyne, lapis lazuli, lazurite, molecular dynamics, resonance Raman spectroscopy, sodalite group, sulfur radical, ultramarine blue pigment

Introduction

Sodalite group minerals, including lazurite $Na_7Ca(Al_6Si_6O_{24})(SO_4)^{2-}(S_3)^-\cdot H_2O$ (Sapozhnikov 2021) and haüyne $Na_{4.5}Ca_2K[Al_6Si_6O_{24}](SO_4)_{1.5}(OH)_{0.5}$ (Hassan and Grundy 1991), are members

of the feldspathoid family. Feldspathoids share an aluminosilicate framework consisting of six-membered rings of Si- and Al-centered tetrahedra. The sodalite group is characterized by sodalite-type (ABC) stacking sequence of aluminosilicate layers and the presence of sodalite (β) cages that can accommodate a variety of cations, anions, and neutral molecules (Sapozhnikov 2021), including a number of sulfur species (Table 1). Of these, the S_3^- and S_2^- radicals deserve special attention for two reasons. First, the sodalite cage is one of the few environments in which these sulfur species can be stabilized at ambient temperature. In geologic fluids, for instance, sulfur radicals become stable only around 200 ˚C (Pokrovski and Dubrovinsky 2011). Second, sulfur radicals are chromophores. Whereas the S_3^- radical is a blue chromophore (Chivers 1974) that made lapis lazuli a highly prized gemstone of the Sumerian and Egyptian antiquity (Gaetani et al. 2004) and the ultramarine blue made from lazurite a desired pigment in both Asia and Europe since the 7th–8th century AD (Gettens 1938)(Gaetani et al. 2004), the S_2^- radical is a yellow chromophore and the increasing S_2^-/S_3^- ratio was found to be responsible for greenish shades and eventually green color of ultramarine pigments (Clark and Cobbold 1978)(Reinen and Lindner 1999). Just like lazurite, blue crystals of haüyne also owe their color to S_3^- radicals (Caggiani et al. 2022).

Given that the identification of sulfur radicals may be hindered by their low concentrations, we decided to employ Raman spectroscopy in the search for sulfur bearing species and take advantage of the rigorous Raman resonance effect shown by sulfur radicals (Clark and Franks 1975)(Clark and Cobbold 1978)(Clark and Dines 1986)(Picquenard et al. 1993). Furthermore, we investigated the enigmatic ~485 cm^{-1} band found previously in Raman spectra of lazurite and haüyne collected with a 458 nm excitation, which was invisible in spectra

This is the peer-reviewed, final accepted version for American Mineralogist, published by the Mineralogical Society of America.
The published version is subject to change. Cite as Authors (Year) Title. American Mineralogist, in press.
DOI: https://doi.org/10.2138/am-2022-8655. http://www.minsocam.org/

collected with a 532 nm excitation and was suggested to be related to the ν_1 band of S_2^- radical (Caggiani et al. 2014).

Locality	Sulfur species	Analytical method	Reference
Lazurite			
Afghanistan Baffin Island, Nunavut, Canada	Sulfate SO_4^{2-} Monosulfide S^{2-}	XRD	(Hassan et al. 1985)
Pamir, Tajikistan	Sulfate SO_4^{2-} S_3^- radical S_2^- radical	Raman, UV-Vis, IR, EPR	(Ostroumov et al. 2002)
Afghanistan Baffin Island, Nunavut, Canada	Sulfate SO_4^{2-} (ma) Monosulfide S^{2-} bound to Na (mi) Elemental sulfur S (mi) Polysulfide (mi)	XANES, XPS	(Fleet et al. 2005)
Malo-Bystrinskoe Deposit, Lake Baikal Region, Russia	Sulfate SO_4^{2-} (ma) Polysulfide (ma) Sulfite SO_3 (mi) Monosulfide S^{2-} (mi) Thiosulfate S_2O_3 (mi) Elemental sulfur S (mi)	XANES, XP	(Tauson et al. 2012)
Badakhshan, Afghanistan	Sulfate SO_4^{2-} S_3^- radical S_2^- radical	Raman	(Caggiani et al. 2014)
Many localities	Sulfate SO_4^{2-} S_3^- and/or S_2^- radical S_2^- radical	XANES	(Gambardella et al. 2016)
Malo-Bystrinskoe Deposit, Lake Baikal Region, Russia	Sulfate SO_4^{2-} (ma) S_3^- radical (ma) Monosulfide S^{2-} (mi, not detected directly)	IR, Raman, EPR, XPS	(Sapozhnikov 2021)
Haüyne			
Sacrafano, Italy	Sulfate SO_4^{2-}	XRD	(Hassan and Grundy 1991)
Toppo San Paolo, Italy Near Mount Vulture volcano, Italy	Sulfate SO_4^{2-} S_3^- radical S_2^- radical	Raman	(Caggiani et al. 2014)
Toppo San Paolo, Italy Melfi, Italy	Sulfate SO_4^{2-} S_3^- radical S_2^- radical	Raman	(Caggiani et al. 2022)

Table 1. Sulfur species in lazurite and haüyne. ma = major phase, mi = minor phase, EPR = electron paramagnetic resonance spectroscopy, IR = Infrared spectroscopy, UV-Vis = Ultraviolet-visible spectroscopy, XANES = X-ray absorption near-edge structure, XPS = X-ray photoelectron spectroscopy, XRD = X-ray diffraction.

Methods

Samples

Raman spectra were collected on naturally occurring lazurite and haüyne samples provided by the Natural History Museum, Geneva, Switzerland, and ultramarine blue pigments purchased from Kremer Pigmente, Germany. The origin of lazurites is as follows: specimen number

003.084 Baikal, Russia; 376.002 Tunnel Mt Cenis, Savoie, France; 397.041 Badakhstan, Kabul, Afghanistan; 425.086 Brazil; and 431.065 Sierra d'Ovalle, Coquimbo, Chile. The origin of haüynes is as follows: 333.049 Mount Vesuvius, Italy and 332.018 Laachersee, Eifel, Germany. The pigments analyzed were: 45000 Ultramarine blue, very dark; 45010 Ultramarine blue, dark; 45020 Ultramarine blue, reddish; 45030 Ultramarine blue, greenish extra; 45040 Ultramarine blue, greenish light; and 45080 Ultramarine blue, light.

Diffuse reflectance spectroscopy

Diffuse reflectance spectra were collected using a UV-visible spectrometer (V-670, JASCO) coupled with an integrating sphere accessory (ARSN-733, JASCO) at the Department of Physical Chemistry, University of Geneva. Each mineral powder sample was mixed with KBr (ca. 1 wt% of a sample in KBr) for the preparation of a 13 mm circular pellet (Specac hydraulic press was used). The pellet was then mounted on the sample holder of the integrated sphere and the diffuse reflectance spectra were measured. Blank KBr pellet was used for obtaining the background spectrum. The measured reflectance (R) was converted to absorbance (A) by calculating $A = -logR$.

Raman spectroscopy

Raman spectra collected with 405 and 532 nm excitations were acquired using a confocal LabRAM HR Evolution (HORIBA Scientific) Raman spectrometer with 800 mm focal length at

the Department of Earth Sciences, University of Geneva. To emphasise the enhancement of S_2^- and S_3^- bands due to the resonance effect, spectra were also collected with a 785 nm excitation using a Renishaw inVia Raman spectrometer with 250 mm focal length at the Natural History Museum of Geneva. However, the interpretation of previously observed spectral features of lazurite in spectra collected with a 785 nm excitation (e.g., González-Cabrera et al. 2022) is beyond the scope of the current study. Both spectrometers were calibrated using the 521 cm^{-1} line of silicon.

The LabRAM spectrometer was equipped with a liquid nitrogen cooled, back illuminated Symphony II CCD detector (1024×256 pixel) and an Olympus BXFM microscope with a motorized XYZ sample stage. The spectral resolution was ~0.5 cm^{-1}. A grating of 1800 lines/mm and a confocal pinhole of 100 μm were employed. A TopMode 405 laser source (Toptica Photonics) with a wavelength of 405 nm and a Torus 532 laser source (Laser Quantum) with a wavelength of 532 nm were used for excitation. The spectra were acquired in backscattering geometry using either an Olympus MPlan N 100× objective with numerical aperture of 0.90 and working distance of 0.21 mm (for lazurites and pigments) or an Olympus LMPlanFL N 50× long working distance objective with numerical aperture of 0.50 and working distance of 10.6 mm (for haüynes).

The Renishaw spectrometer was equipped with a Peltier cooled CCD detector (400×576 pixel) and a DM Leica 2500 microscope with a motorized XYZ sample stage. The spectral resolution was ~1.5 cm^{-1}. A grating of 1200 lines/mm and a slit of 65 μm were employed. A HPNIR785 diode laser source (Renishaw) with a wavelength of 785 nm was used for excitation. The spectra were acquired in backscattering geometry using a Leica 50× long working distance objective with numerical aperture of 0.55 and working distance of 8 mm.

For each spectrum collected with the 405 nm and 532 nm lasers, three accumulations of 10 s each were taken in multiple spectral windows resulting in a final range of 150–5000 cm^{-1}. In addition, spectra with ten accumulations of 10 s each were taken in the spectral window of 400–700 cm^{-1}. To prevent the saturation of the CCD detector while collecting spectra of lazurites and to prevent the burning of pigments, a power filter of 10% was also applied for these measurements, reducing the maximum power of ~30 mW measured at the sample to ~3 mW.

For each spectrum collected with the 785 nm laser, ten accumulations of 10 s each were taken in the spectral window of 400–1200 cm^{-1}. To prevent the saturation of the CCD detector, power filters of 1, 5, or 10% were applied for the measurement of lazurites and haüynes and to prevent the burning of samples, a power filter of 0.1% was applied for the measurement of pigments, significantly reducing the maximum power of ~300 mW measured at the sample.

Ab initio molecular dynamics

Molecular dynamics simulations were performed using the VASP package (Kresse and Hafner 1993)(Kresse and Joubert 1999). The interatomic forces were computed using the planar augmented wavefunction method (Blöchl 1994). The generalized gradient approximation (Perdew et al. 1996) was used to describe the exchange correlation term of the energy. The electronic density and wavefunctions were computed using the sampling of the reciprocal space in the Γ point. The simulations were run for at least 30 picoseconds with a time step of 1 femtosecond.

The analysis of the simulations was completed using the UMD package (Caracas et al. 2021a, 2021b). The geometry of the S–S bonds was monitored computing the pair distribution

functions (PDFs). The first minimum of the PDFs yields the maximum bond distance and in a fluid description corresponds to the radius of the first coordination sphere. This distance was used to asses the speciation within the polysulfide ions. The vibrational spectra were obtained as the Fourier transform of the self-correlation function of the atomic velocities.

Results and discussion

Raman resonance means that when a molecule is excited with a laser with a frequency close to the maximum of an allowed electronic transition, the Raman spectra are characterized by an enhancement in the intensity of a totally symmetric fundamental of the scattering molecule and by high-intensity overtone progressions in this fundamental (Holzer et al. 1970)(Nafie et al. 1971)(Clark and Franks 1975). Whereas the S_3^- radical shows a broad absorption band with a maximum around 610-620 nm due to the $X^2B_1 \rightarrow C^2A_2$ transition (Chivers and Drummond 1972)(Seel et al. 1977)(Clark and Cobbold 1978)(Reinen and Lindner 1999)(Linguerri et al. 2008)(Shnitko et al. 2008), the S_2^- radical shows an absorption band with a maximum around 390-400 nm due to the $^2\Pi_g \rightarrow {}^2\Pi_u$ transition (Figure 1)(Holzer et al. 1969)(Clark and Cobbold 1978). Therefore, we employed 405 nm excitation that lies inside the absorbance band of the S_2^- radical, 532 nm excitation that lies inside the absorbance band of the S_3^- radical, and 785 nm excitation that lies outside the absorbance bands of either radicals (Figure 1) to collect Raman spectra of five lazurites, two haüynes, and six synthetic ultramarine blue pigments to identify the sulfur species present in each (see Supplementary material). Representative spectra of these are shown in Figures 2, 3, and 4, respectively. In the following section, the observed bands of sulfur species are discussed.

This is the peer-reviewed, final accepted version for American Mineralogist, published by the Mineralogical Society of America.
The published version is subject to change. Cite as Authors (Year) Title. American Mineralogist, in press.
DOI: https://doi.org/10.2138/am-2022-8655. http://www.minsocam.org/

Sulfate bands. The $\nu_1(SO_4^{2-})$ bands in the 976 – 1003 cm^{-1} region, corresponding to the S–O stretching mode (Choi and Lockwood 1989), are visible in most lazurite and haüyne spectra (Figures 2 and 3), whereas the $\nu_2(SO_4^{2-})$ band at 437 cm^{-1}, corresponding to the S–O bending mode (Choi and Lockwood 1989) is only visible in the spectra of haüyne (Figure 3). In haüyne spectra, up to three bands appear in the sulfate region, likely representing different coordination environments in the sodalite (β) cages. In a recent study, five bands related to the silicate and sulfate groups have been documented in the 950-1030 cm^{-1} spectral region in haüyne originating from the Mount Vulture area in Italy (Caggiani et al. 2022). Sulfate bands are absent in spectra of ultramarine blues.

S_3^- bands. The $\nu_1(S_3^-)$ band at ~546 cm^{-1}, corresponding to the symmetric S–S stretching mode (Holzer et al. 1969)(Chivers and Drummond 1972)(Clark and Franks 1975), is visible in all lazurite, haüyne, and ultramarine blue spectra. Given that the 532 nm excitation line lies inside the absorbance band of the S_3^- radical (Figure 1), spectra collected with the 532 nm excitation show a strong enhancement of the intensity of the $\nu_1(S_3^-)$ band, the $\nu_2(S_3^-)$ band at ~258 cm^{-1}, corresponding to the symmetric S–S bending mode (Chivers and Drummond 1972)(Clark and Franks 1975), and the $\nu_3(S_3^-)$ band at ~582 cm^{-1}, corresponding to the anti-symmetric S–S stretching mode (Figures 2, 3, and 4)(Table 2)(Ledé et al. 2007). The 532 nm spectra also show $n\nu_1$ and $\nu_2 + n\nu_1$ progressions of the $\nu_1(S_3^-)$ band (Figures 2, 3, and 4)(Table 2).

S_2^- bands. The position of the $\nu_1(S_2^-)$ band, corresponding to the symmetric S–S stretching mode (Holzer et al. 1969)(Clark and Franks 1975), coincides with that of the $\nu_3(S_3^-)$ band (Ledé et al. 2007). Given that the concentration of S_3^- in the studied materials is high enough that its spectral features are visible even in the non-resonant Raman spectra (i.e., those collected with 405 and 785 nm excitations), a small portion of the ~582 cm^{-1} spectral feature in

197 spectra collected with the 405 nm excitation, correspond to the $\nu_3(S_3^-)$ band. The dominant
198 contribution of the ~582 cm^{-1} spectral feature is the $\nu_1(S_2^-)$ band, because the 405 nm excitation
199 line lies inside the absorbance band of the S_2^- radical. The 405 nm spectra of lazurites, haüynes,
200 and ultramarine blues indeed show a greatly enhanced $\nu_1(S_2^-)$ band and its $n\nu_1$ progression
201 (Figures 2, 3, and 4)(Table 2).

202 *The 481, 443, and 223 cm^{-1} bands.* Bands at 481 and 223 cm^{-1}, along with the
203 progressions of the 481 cm^{-1} band appear in four of the five lazurite spectra and in one of the two
204 haüyne spectra collected with the 405 nm excitation (Figures 2 and 3)(Table 2). In addition, a
205 band at 443 cm^{-1} is visible in the spectrum of lazurite form Brazil (Figure 2)(Table 2). These
206 bands are absent in spectra of ultramarine blues (Figure 4). This observation is consistent with
207 earlier studies in which no ~480 cm^{-1} band has been observed in spectra of synthetic pigments
208 collected with a 405 nm laser (Del Federico et al. 2006). The 481 cm^{-1} band has already been
209 reported in spectra of lazurite and haüyne collected with a 458 nm excitation, but was absent in
210 spectra collected with a 532 nm laser and has not been assigned to any species (Caggiani et al.
211 2014). These previous observations are consistent with ours and suggest that another
212 chromophore species with an absorption maximum in/near the 400-450 nm region is responsible
213 for the 481 and 223 cm^{-1} bands. In all lazurite samples, upon subsequent spectra acquisitions
214 from the same irradiated volume, the 481 and 223 cm^{-1} bands and the progression of the 481 cm^{-1}
215 band rapidly lose intensity (Figures 5 and 6). Simultaneously, the area of $\nu_1(S_2^-)$ band and its
216 progression gradually increases (Figures 5 and 6). The breakdown of the 481 and 223 cm^{-1} bands
217 can be further accelerated with increasing laser power as shown in time profiles employing filters
218 that reduce the maximum power to 5, 10, 25, and 50% (Figure 7).
219

This is the peer-reviewed, final accepted version for American Mineralogist, published by the Mineralogical Society of America.
The published version is subject to change. Cite as Authors (Year) Title. American Mineralogist, in press.
DOI: https://doi.org/10.2138/am-2022-8655. http://www.minsocam.org/

Our observations indicate a laser-induced reaction of a S-bearing species to S_2^-. Indeed, visible light of suitable wavelengths can lead to the breakage of S–S bonds in polysulfur compounds (Steudel and Chivers 2019). The S-bearing species in question has its strongest Raman bands at 481 and 223 cm^{-1}, an absorption maximum in/near the 400-450 nm region, must contain at least three sulfur atoms to exhibit two Raman bands and must not contain more than six sulfur atoms to fit the sodalite (β) cages of lazurite and haüyne. The S_4^{2-} polysulfide ion fulfills all these criteria: its ν_1 symmetric S–S stretching vibration is at 480 cm^{-1} (Janz et al. 1976)(Chivers and Lau 1982), its absorption maximum is at ~420-430 nm (Martin et al. 1973)(Badoz-Lambling et al. 1976) and is small enough to be accommodated in the β cages. Furthermore, the Raman-active vibrational frequencies calculated by Tossell (2012) at the cc-pvTZ CCSD PCM level for S_4^{2-} (482 cm^{-1} for the strongest, 228, 449, and 504 cm^{-1}), are in close agreement with those observed by us. The laser-induced decomposition of S_4^{2-} likely produces S_2^- according to the reaction:

$$S_4^{2-} \rightarrow 2S_2^-$$

Indeed, the dissociation of polysulfides to sulfur radicals upon heating or the dimerization of sulfur radicals upon cooling have been observed previously in dissolution experiments of alkali polysulfides (Giggenbach 1968)(Seel et al. 1977). Moreover, S_4^{2-} has already been successfully trapped in synthetic sodalite structure materials (Ruivo et al. 2018)(Lim et al. 2018). Finally, S_4^{2-} has been suggested as a species contributing to an envelope of peaks between 2470 and 2475 eV in the XANES spectra of lazurite (Gambardella et al. 2016). In contrast to lazurite, the ν_1 band of S_4^{2-} in haüyne is only slightly affected by the laser beam, even when using full laser power (Figure 8). Moreover, there is no growth of the ν_1 band of S_2^- observed that would indicate the decomposition of S_4^{2-}. S_4^{2-} is therefore much more stable in haüyne than lazurite.

Ab initio molecular dynamics. To confirm the nature and stability of the polysulfide ions trapped in the sodalite (β) cages of lazurite, we ran a series of *ab initio* molecular dynamics simulations at 300 K. Lazurite host minerals were modeled using a cubic model host with $[Na_8Al_6Si_6O_{12}]^{2+}$ stoichiometry within either one unit cell or a 2x2x2 supercell. The S_3^{2-}, S_4^{2-} and S_6^{2-} polysulfide groups were placed inside the large cages of the model lazurite in linear geometry parallel to the diagonals of the cube. Using the first minimum of the PDFs (Figure 9) as the criterion for bonding, the simulations show the large remarkable stability of the S_3^{2-} linear group. In the S_3^{2-} bearing cells, the linear group dominates the sulfur speciation by up to 80%, and the rest of the time it is split into an S_2 group and one isolated S atom. But the lifetime of the isolated S_2 + S configuration is less than 30 femtoseconds. In the S_4^{2-} bearing cells, the complete linear group represents about 6% of the total sulfur population and the rest of the time it is split into two S_2 molecules. Finally, the S_6^{2-} polysulfide group is split into two S_3 linear groups for the entire duration of the simulation. The vibrational analysis reveals peaks corresponding to the S_2 and S_3 groups, but fails to find any peak corresponding to the S_4^{2-} peak. This is due to the low concentration of the S_4 linear group, which is not enough to leave a signature in the total vibrational spectrum. The actual positions of the S_2 and S_3 peaks are highly dependent on the density of the simulated material and they appear shifted with respect to experiments. Only the relative S_2/S_3 positions are consistent with experiments.

Simulations that started with tetrahedral S_4^{2-} groups saw their immediate dissociation in two S_2^- molecules. The same phenomenon appeared in simulations of Na_2S_4, or CaS_4. Moreover, if the density of these systems is too low, the DFT simulations tend to dissociate the molecules and transform them into an amorphous phase, similar to a gas.

This is the peer-reviewed, final accepted version for American Mineralogist, published by the Mineralogical Society of America.
The published version is subject to change. Cite as Authors (Year) Title. American Mineralogist, in press.
DOI: https://doi.org/10.2138/am-2022-8655. http://www.minsocam.org/

Geometry of the S_4^{2-} polysulfide ion and the assignment of observed bands. The S_4^{2-} polysulfide ion may exist in several geometries, including chain (Tegman 1973), ring (Mealli et al. 2008)(Poduska et al. 2009), and branched geometry (Lim et al. 2018). An example of a chain geometry is solid Na_2S_4 (Tegman 1973) that has two symmetric stretching modes: a ν_1 symmetric S–S stretching vibration, involving a terminal S atom at 482 cm^{-1} and a ν_2 symmetric S–S stretching vibration involving two central S atoms at 445 cm^{-1} (Janz et al. 1976). While in the lazurite from Brazil there is a prominent shoulder present at ~443 cm^{-1} that may be associated with the ν_2 symmetric S–S stretching vibration, no ~445 cm^{-1} shoulder is present in the lazurite form Russia (Figure 6). The absence of the ν_2 symmetric S–S stretching vibration in the lazurite form Russia may indicate the presence of S_4^{2-} rings rather than linear S_4^{2-} units, in which all S–S bonds are equivalent leading to only one symmetric S–S stretching vibration. MD simulation indicates the preference of S_4^{2-} to form linear units rather than rings and therefore we propose a chain geometry of S_4^{2-} polysulfide ion in the cage, and follow the assignment of vibrational modes proposed by Janz et al. (1976)(Table 2). However, we do not discard the possibility of the existence of S_4^{2-} rings in the sodalite (β) cages of lazurite and haüyne.

Other S-bearing species. Several additional bands appear in the 230-280 cm^{-1} and 600-650 cm^{-1} regions of certain lazurite and haüyne spectra that may be associated with other S-bearing species. However, the assignment of these is not trivial and is beyond the scope of this study.

Vibrational mode	Sample												Reference for assignment
	Lazurite (Russia)			Lazurite (Brazil)			Haüyne (Italy)			Synthetic ultramarine blue			
	Laser wavelength (nm)												
	405	532	785	405	532	785	405	532	785	405	532	785	
S_2^-													
ν_1 symmetric S–S stretching	582			581			586			583			(Holzer et al. 1969)
$2\nu_1$ overtone	1163			1162			1171			1164			(Holzer et al. 1969)
$3\nu_1$ overtone	1740			1739						1736			(Holzer et al. 1969)
$4\nu_1$ overtone	2314			2313						2310			(Clark and Franks 1975)
$5\nu_1$ overtone	2882			2879						2879			
$6\nu_1$ overtone	3448			3447						3445			
$7\nu_1$ overtone										3967			

This is the peer-reviewed, final accepted version for American Mineralogist, published by the Mineralogical Society of America.
The published version is subject to change. Cite as Authors (Year) Title. American Mineralogist, in press.
DOI: https://doi.org/10.2138/am-2022-8655. http://www.minsocam.org/

$8\nu_1$ overtone										4516			
S_3^-													
ν_1 symmetric S–S stretching	546	546	546	545	545	545	547	547	547	545	545	545	(Holzer et al. 1969)
$2\nu_1$ overtone		1093			1089			1100			1098		(Holzer et al. 1969)
$3\nu_1$ overtone		1643			1638						1645		(Holzer et al. 1969)
$4\nu_1$ overtone		2187			2182						2181		(Holzer et al. 1969)
$5\nu_1$ overtone		2731			2723						2728		(Holzer et al. 1969)
$6\nu_1$ overtone		3264			3256						3266		(Holzer et al. 1969)
$7\nu_1$ overtone		3795			3789						3797		
$8\nu_1$ overtone		4317			4314						4311		
ν_2 symmetric S–S bending		258			258			260			254		(Chivers and Drummond 1972)
$\nu_1+\nu_2$ overtone		805			805			813			801		(Clark and Franks 1975)
$2\nu_1+\nu_2$ overtone		1355			1353						1354		(Clark and Franks 1975)
$3\nu_1+\nu_2$ overtone		1895			1898						1895		(Clark and Franks 1975)
$4\nu_1+\nu_2$ overtone		2448			2441								
$5\nu_1+\nu_2$ overtone		2986			2977								
$6\nu_1+\nu_2$ overtone		3512			3509								
$7\nu_1+\nu_2$ overtone		4049			4046								
ν_3 antisymmetric S–S stretching		585			582			587					(Ledé et al. 2007)
S_4^{2-}													
ν_1 symmetric $S_{central}$–$S_{terminal}$ stretching	483			481			483						(Janz et al. 1976)
$2\nu_1$ overtone	962			960									
$3\nu_1$ overtone	1439			1442									
$4\nu_1$ overtone				1921									
$5\nu_1$ overtone				2394									
ν_2 symmetric $S_{central}$–$S_{central}$ stretching				443									(Janz et al. 1976)
ν_3 symmetric S–S bending	222			223									(Janz et al. 1976)
$\nu_1+\nu_3$ overtone	709			712									
$3\nu_1+\nu_3$ overtone				1685									

Table 2. Observed vibrational frequencies of S_2^- and S_3^- radicals and the S_4^{2-} polysulfide ions in lazurite, haüyne and ultramarine blue.

Implications

The spectral features of the S_4^{2-} polysulfide ion are only visible in Raman resonance spectra collected with 405 nm excitation that lies inside the absorbance band of S_4^{2-}. The absence of these peak in the MD simulations and in the observations with other laser wavelengths suggests a strong Raman resonance effect. This underlines that Raman resonance spectroscopy a powerful method to detect very low concentrations of S_4^{2-} (and other polysulfides), which are below the detection limit of Raman spectra collected with different excitations or other conventional analytical techniques (e.g., X-ray powder diffraction).

The intensity of the Raman bands of S_2^- and S_3^- radicals is also very strongly enhanced when these species are measured with excitations that lie inside their respective absorption bands, showing that resonance Raman spectroscopy is a powerful qualitative tool to detect very

small amounts of sulfur radicals. However, in studies aiming to measure the concentration of sulfur radicals in solutions, Raman resonance should be eliminated and the quantification of sulfur radicals should only be attempted with excitations lying outside their respective absorption bands (Schmidt and Seward 2017). This is critically important for studies aiming to quantify sulfur radical species in high-pressure-temperature fluids resembling geologic fluids and assess their role in metal mobilization, transport, and ore deposit formation. Hackmanite, a variety of sodalite, has been suggested to contain S_2^- radicals (Müller 2017). To confirm this suggestion and to detect polysulfide species in different minerals and materials, resonance Raman spectroscopy seem to be the ideal analytical technique.

The laser induced decomposition of the S_4^{2-} polysulfide ion into two S_2^- radicals in lazurite was observed even while using a 5% laser power filter (corresponding to ~1.5 mW at the sample). Sulfur species are known for their sensitivity to visible light and high probability for beam damage (Steudel and Chivers 2019). Checks for laser induced reactions and damage and the use of low laser power is therefore recommended when analyzing polysulfides.

Given the post-entrapment and post-cooling immobility of most sulfur species in the sodalite cages of lazurite and haüyne, their ratios can potentially reflect the chemical state of metasomatizing fluids (Tauson et al. 2011). The distinct $SO_4^{2-}/(S_2^- + S_4^{2-})/S_3^-$ ratios of the analyzed lazurite samples may also provide hints on the provenance of lazurite used to make ultramarine blue pigments.

Finally, there is considerable interest in entrapping S_4^{2-} into synthetic sodalite structure materials, because these show high external quantum efficiency values, large Stokes shifts, and thermal stability, and can find applications in light down-conversion systems or as phosphors in

lighting devices (Ruivo et al. 2018). S_4^{2-} in haüyne was found surprisingly stable in comparison with lazurite, making haüyne a potentially interesting host material for S_4^{2-} entrapment.

Acknowledgements

Edwin Gnos from the Natural History Museum of Geneva is acknowledged for lending the lapis lazuli and haüyne samples. We thank Thomas Bürgi from University of Geneva for letting us use his diffuse reflectance spectroscopy setup. Arnulf Rosspeintner and Jafar Afshani from University of Geneva are acknowledged for their assistance with diffuse reflectance measurements. We thank the anonymous reviewers and the associate editor Jianwei Wang for their helpful comments and suggestions. SF and ZZ acknowledges the European Union because this project was funded by the European Research Council (ERC) under the European Union's Horizon 2020 research and innovation programme (grant agreement no. 864792, ERC Consolidator Grant OXYGEN to ZZ). RC acknowledges support from the European Research Council (ERC) under the European Union's Horizon 2020 research and innovation programme (grant agreement no. 681818 – IMPACT to RC), the Research Council of Norway, project number 223272 and through project HIDDEN 325567, and access to supercomputing facilities via the eDARI stl2816 grants, the PRACE RA4947 and RA240046 grant, and the Uninet2 NN9697K grant.

References

Badoz-Lambling, J., Bonnaterre, R., Cauquis, G., Delamar, M., and Demange, G. (1976) La

reduction du soufre en milieu organique. Electrochimica Acta, 21, 119–131.

Blöchl, P.E. (1994) Projector augmented-wave method. Physical Review B, 50, 17953–17979.

Caggiani, M.C., Acquafredda, P., Colomban, P., and Mangone, A. (2014) The source of blue colour of archaeological glass and glazes: the Raman spectroscopy/SEM-EDS answers. Journal of Raman Spectroscopy, 45, 1251–1259.

Caggiani, M.C., Mangone, A., and Acquafredda, P. (2022) Blue coloured haüyne from Mt. Vulture (Italy) volcanic rocks: SEM-EDS and Raman investigation of natural and heated crystals. Journal of Raman Spectroscopy, 53, 956–968.

Caracas, R., Kobsch, A., Solomatova, N. V., Li, Z., Soubiran, F., and Hernandez, J.A. (2021a) Analyzing melts and fluids from Ab initio molecular dynamics simulations with the UMD package. Journal of Visualized Experiments, 2021, 1–20.

——— (2021b) Analyzing melts and fluids from Ab initio molecular dynamics simulations with the UMD package. Journal of Visualized Experiments, 2021.

Chivers, T. (1974) Ubiquitous trisulphur radical ion S3-. Nature, 252, 32–33.

Chivers, T., and Drummond, I. (1972) Characterization of the Trisulfur Radical Anion S3- in Blue Solutions of Alkali Polysulfides in Hexamethylphosphoramide. Inorganic Chemistry, 11, 2525–2527.

Chivers, T., and Lau, C. (1982) Raman Spectroscopic Identification of the S4N- and S3- Ions in Blue Solutions of Sulfur in Liquid Ammonia. Inorganic Chemistry, 21, 453–455.

Choi, B.-K., and Lockwood, D.. (1989) Raman spectrum of Na2SO4 (Phase V). Solid State Communications, 72, 133–137.

Clark, B.R.J.H., and Dines, T.J. (1986) Resonance Raman Spectroscopy, and Its Application to Inorganic Chemistry. Angewandte Chemie - International Edition, 25, 131–158.

Clark, R.J.H., and Cobbold, D.G. (1978) Characterization of Sulfur Radical Anions in Solutions of Alkali Polysulfides in Dimethylformamide and Hexamethylphosphoramide and in the Solid State in Ultramarine Blue, Green, and Red. Inorganic Chemistry, 17, 3169–3174.

Clark, R.J.H., and Franks, M.L. (1975) The resonance Raman spectrum of ultramarine blue. Chemical Physics Letters, 34, 69–72.

Del Federico, E., Shöfberger, W., Schelvis, J., Kapetanaki, S., Tyne, L., and Jerschow, A. (2006) Insight into Framework Destruction in Ultramarine Pigments. Inorganic Chemistry, 45, 1270–1276.

Fleet, M.E., Liu, X., Harmer, S.L., and Nesbitt, H.W. (2005) Chemical state of sulfur in natural and synthetic lazurite by S K-edge XANES and X-ray photoelectron spectroscopy. The Canadian Mineralogist, 43, 1589–1603.

Gaetani, M.C., Santamaria, U., and Seccaroni, C. (2004) The use of Egyptian blue and lapis lazuli in the middle ages: The wall paintings of the San Saba church in Rome. Studies in Conservation, 49, 13–22.

Gambardella, A.A., Schmidt Patterson, C.M., Webb, S.M., and Walton, M.S. (2016) Sulfur K-edge XANES of lazurite: Toward determining the provenance of lapis lazuli. Microchemical Journal, 125, 299–307.

Gettens, R.J. (1938) The materials in the wall paintings of Bamiyan, Afghanistan. Technical studies in the field of the fine arts, 6, 186–193.

Giggenbach, W. (1968) On the nature of blue sulfur solutions. Journal of Inorganic and Nuclear Chemistry, 30, 3189–3201.

González-Cabrera, M., Wieland, K., Eitenberger, E., Bleier, A., Brunnbauer, L., Limbeck, A., Hutter, H., Haisch, C., Lendl, B., Domínguez-Vidal, A., and others (2022) Multisensor

391 hyperspectral imaging approach for the microchemical analysis of ultramarine blue
392 pigments. Scientific Reports, 12, 707.
393 Hassan, I., and Grundy, H.D. (1991) The crystal structure of hauyne at 293 and 153 K. The
394 Canadian Mineralogist, 29, 123–130.
395 Hassan, I., Peterson, R.C., and Grundy, H.D. (1985) The Structure of Lazurite, Ideally
396 Na6Ca2(Al6Si6O24)S2, a Member of the Sodalite Group. Acta Crystallographica, C41,
397 827–832.
398 Holzer, W., Murphy, W.F., and Bernstein, H.J. (1969) Raman Spectra of Negative Molecular
399 Ions Doped in Alkali Halide Crystals. Journal of Molecular Spectroscopy, 32, 13–23.
400 ——— (1970) Resonance Raman Effect and Resonance Fluorescence in Halogen Gases. The
401 Journal of Chemical Physics, 52, 399–407.
402 Janz, G.J., Downey, J.R., Roduner, E., Wasilczyk, G.J., Coutts, J.W., and Eluard, A. (1976)
403 Raman Studies of Sulfur-Containing Anions in Inorganic Polysulfides. Sodium. Inorganic
404 Chemistry, 15, 1759–1763.
405 Kresse, G., and Hafner, J. (1993) Ab initio molecular dynamics for liquid metals. Physical
406 Review B, 47, 558–561.
407 Kresse, G., and Joubert, D. (1999) From ultrasoft pseudopotentials to the projector augmented-
408 wave method. Physical Review B - Condensed Matter and Materials Physics, 59, 1758–
409 1775.
410 Ledé, B., Demortier, A., Gobeltz-Hautecœur, N., Lelieur, J.P., Picquenard, E., and Duhayon, C.
411 (2007) Observation of the ν3 Raman band of S3- inserted into sodalite cages. Journal of
412 Raman Spectroscopy, 38, 1461–1468.
413 Lim, H.S., Heo, N.H., and Seff, K. (2018) Disproportionation of an Element in a Zeolite. III.

Crystal Structure of a High-Temperature Sulfur Sorption Complex of Zeolite LTA Containing Two New Ions: Perthiosulfite, S42-, and the Trisulfur Cation, S32+. Journal of Physical Chemistry C, 122, 28133–28141.

Linguerri, R., Komiha, N., Fabian, J., and Rosmus, P. (2008) Electronic States of the Ultramarine Chromophore S3-. Zeitschrift fur Physikalische Chemie, 222, 163–176.

Martin, R.P., Doub, W.H., Roberts, J.L., and Sawyer, D.T. (1973) Further Studies of the Electrochemical Reduction of Sulfur in Aprotic Solvents. Inorganic Chemistry, 12, 1921–1925.

Mealli, C., Ienco, A., Poduska, A., and Hoffmann, R. (2008) S42- rings, disulfides, and sulfides in transition-metal complexes: The subtle interplay of oxidation and structure. Angewandte Chemie - International Edition, 47, 2864–2868.

Müller, H. (2017) La fluorite bleuissante de Tignes, Tarentaise, Savoie. Le Règne Minéral, 42–44.

Nafie, L.A., Stein, P., and Peticolas, W.L. (1971) Time ordered diagrams for the resonant Raman effect from molecular vibrations. Chemical Physics Letters, 12, 131–136.

Ostroumov, M., Fritsch, E., Faulques, E., and Chauvet, O. (2002) Etude spectrometrique de la lazurite du Pamir, Tajikistan. Canadian Mineralogist, 40, 885–893.

Perdew, J.P., Burke, K., and Ernzerhof, M. (1996) Generalized gradient approximation made simple. Physical Review Letters, 77, 3865–3868.

Picquenard, E., El Jaroudi, O., and Corset, J. (1993) Resonance Raman spectra of the S3 molecule in sulphur vapour. Journal of Raman Spectroscopy, 24, 11–19.

Poduska, A., Hoffmann, R., Ienco, A., and Mealli, C. (2009) “Half-bonds” in an unusual coordinated S42- rectangle. Chemistry - An Asian Journal, 4, 302–313.

Pokrovski, G.S., and Dubessy, J. (2015) Stability and abundance of the trisulfur radical ion S3- in hydrothermal fluids. Earth and Planetary Science Letters, 411, 298–309.

Pokrovski, G.S., and Dubrovinsky, L.S. (2011) The S3- ion is stable in geological fluids at elevated temperatures and pressures. Science, 331, 1052–1054.

Reinen, D., and Lindner, G.G. (1999) The nature of the chalcogen colour centres in ultramarine-type solids. Chemical Society Reviews, 28, 75–84.

Ruivo, A., Coutino-Gonzalez, E., Santos, M.M., Baekelant, W., Fron, E., Roeffaers, M.B.J., Pina, F., Hofkens, J., and Laia, C.A.T. (2018) Highly Photoluminescent Sulfide Clusters Confined in Zeolites. The Journal of Physical Chemistry C, 122, 14761–14770.

Sapozhnikov, A.N. (2021) On the crystal chemistry of sulfur-rich lazurite, ideally Na7Ca(Al6Si6O24)(SO4)(S3)–·nH2O. American Mineralogist, 106, 226–234.

Schmidt, C., and Seward, T.M. (2017) Raman spectroscopic quantification of sulfur species in aqueous fluids: Ratios of relative molar scattering factors of Raman bands of H2S, HS−, SO2, HSO4−, SO42−, S2O32−, S3− and H2O at ambient conditions and information on changes with pressure and tempe. Chemical Geology, 467, 64–75.

Seel, F., Güttler, H.-J., Simon, G., and Wieckowski, A. (1977) Colored Sulfur Species in EPD-Solvents. Pure and Applied Chemistry, 49, 45–54.

Shnitko, I., Fulara, J., Garkusha, I., Nagy, A., and Maier, J.P. (2008) Electronic transitions of S2- and S3- in neon matrixes. Chemical Physics, 346, 8–12.

Steudel, R., and Chivers, T. (2019) The role of polysulfide dianions and radical anions in the chemical, physical and biological sciences, including sulfur-based batteries. Chemical Society Reviews, 48, 3279–3319.

Tauson, V.L., Sapozhnikov, A.N., Shinkareva, S.N., and Lustenberg, E.E. (2011) Indicative

properties of lazurite as a member of clathrasil mineral family. Doklady Earth Sciences, 441, 1732–1737.

Tauson, V.L., Goettlicher, J., Sapozhnikov, A.N., Mangold, S., and Lustenberg, E.E. (2012) Sulphur speciation in lazurite-type minerals (Na,Ca)8[Al6Si6O24](SO4,S)2 and their annealing products: a comparative XPS and XAS study. European Journal of Mineralogy, 24, 133–152.

Tegman, R. (1973) The Crystal Structure of Sodium Tetrasulphide, Na2S4. Acta Crystallographica, B29, 1463–1469.

Tossell, J.A. (2012) Calculation of the properties of the S3- radical anion and its complexes with Cu+ in aqueous solution. Geochimica et Cosmochimica Acta, 95, 79–92.

List of figures

Figure 1. Diffuse reflectance spectrum of the NHMG425.086 lazurite sample from Brazil showing absorption bands of S_2^- and S_3^- radicals. The 405, 532, and 785 nm excitation lines used in this study are also shown.

Figure 2. Raman spectra of lazurite samples collected with different excitations: a-b) spectra of the NHMG003.084 sample from Baikal, Russia; c-d) spectra of the NHMG425.086 sample from Brazil. In b) and d) spectra collected with the 405 nm excitation were vertically exaggerated and offset relative to the 532 nm spectra.

Figure 3. Raman spectra of the NHMG333.049 haüyne sample from Mount Vesuvius, Italy collected with different excitations. In b) the spectrum collected with the 405 nm excitation was vertically exaggerated and offset relative to the 532 nm spectrum.

Figure 4. Raman spectra of the "45000 Ultramarine blue, very dark" pigment collected with different excitations. In b) the spectrum collected with the 405 nm excitation was vertically exaggerated and offset relative to the 532 nm spectrum.

Figure 5. Spectra showing the laser-induced decomposition of the S_4^{2-} polysulfide ions into S_2^- radicals in lazurite sample NHMG425.086 from Brazil. Both spectra were collected with 405 nm excitation, 50% laser power filter, and for a duration of 1 s. The red spectrum was collected following a 29 s exposure of sample to laser beam, resulting in 30 s of total exposure time.

494

495 Figure 6. a-b) Time profiles showing the gradual, laser-induced decomposition of the S_4^{2-}
496 polysulfide ions into S_2^- radicals in lazurite samples. All spectra were collected with the 405 nm
497 excitation, 10% laser power filter, and for a duration of 10 s. The numbers in the key indicate
498 total exposure times to laser beam. a) sample NHMG003.084 from Baikal, Russia; b) sample
499 NHMG425.086 from Brazil. Note the difference in initial $\nu_1(S_4^{2-})/\nu_1(S_2^-)$ band ratios. c-d)
500 Corresponding changes in peak areas.

501

502 Figure 7. Time profiles showing the effect of laser power expressed as % of maximum power (30
503 mW at the sample) on the gradual, laser-induced decomposition of the S_4^{2-} polysulfide ions into
504 S_2^- radicals in the NHMG425.086 lazurite sample from Brazil collected with the 405 nm
505 excitation and for a duration of 10 s. The numbers in the key indicate total exposure times to
506 laser beam.

507

508 Figure 8. Time profile showing the stability of S_4^{2-} polysulfide ions in the NHMG333.049
509 haüyne sample from Mount Vesuvius, Italy. All spectra were collected with the 405 nm
510 excitation, at full laser power, and for a duration of 10 s. The numbers in the key indicate total
511 exposure times to laser beam.

512

513 Figure 9. S–S pair distribution functions computed for the polysulfide groups trapped in lazurite.
514 The first peak corresponds to the average interatomic bond distance. The first minima (which are
515 marked on the plot) correspond to the radius of the first coordination sphere. Atoms are
516 considered bonded if their distance is less than this radius.

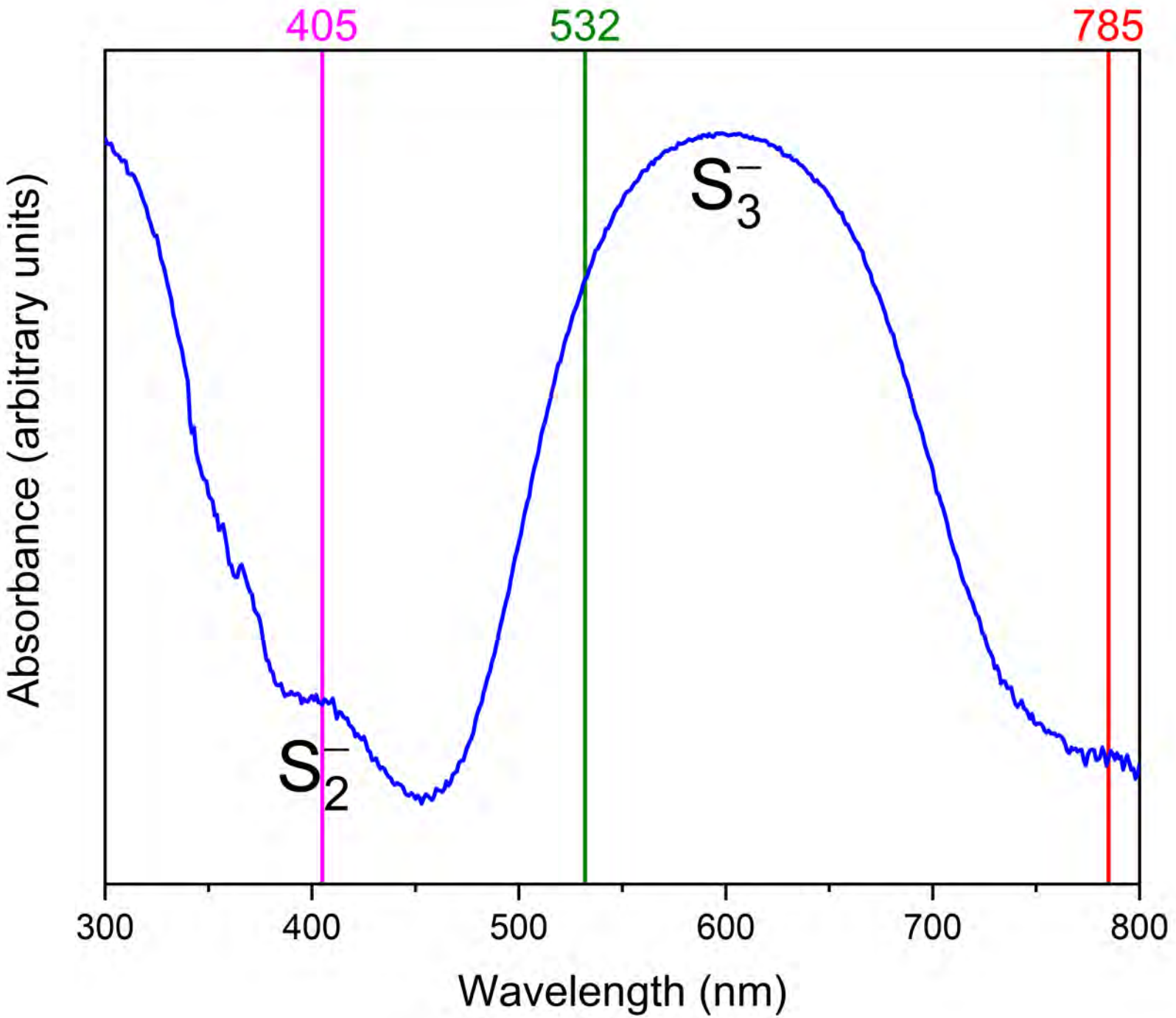
405
532
785
Absorbance (arbitrary units)
S_3^-
S_2^-
300
400
500
600
700
800
Wavelength (nm)

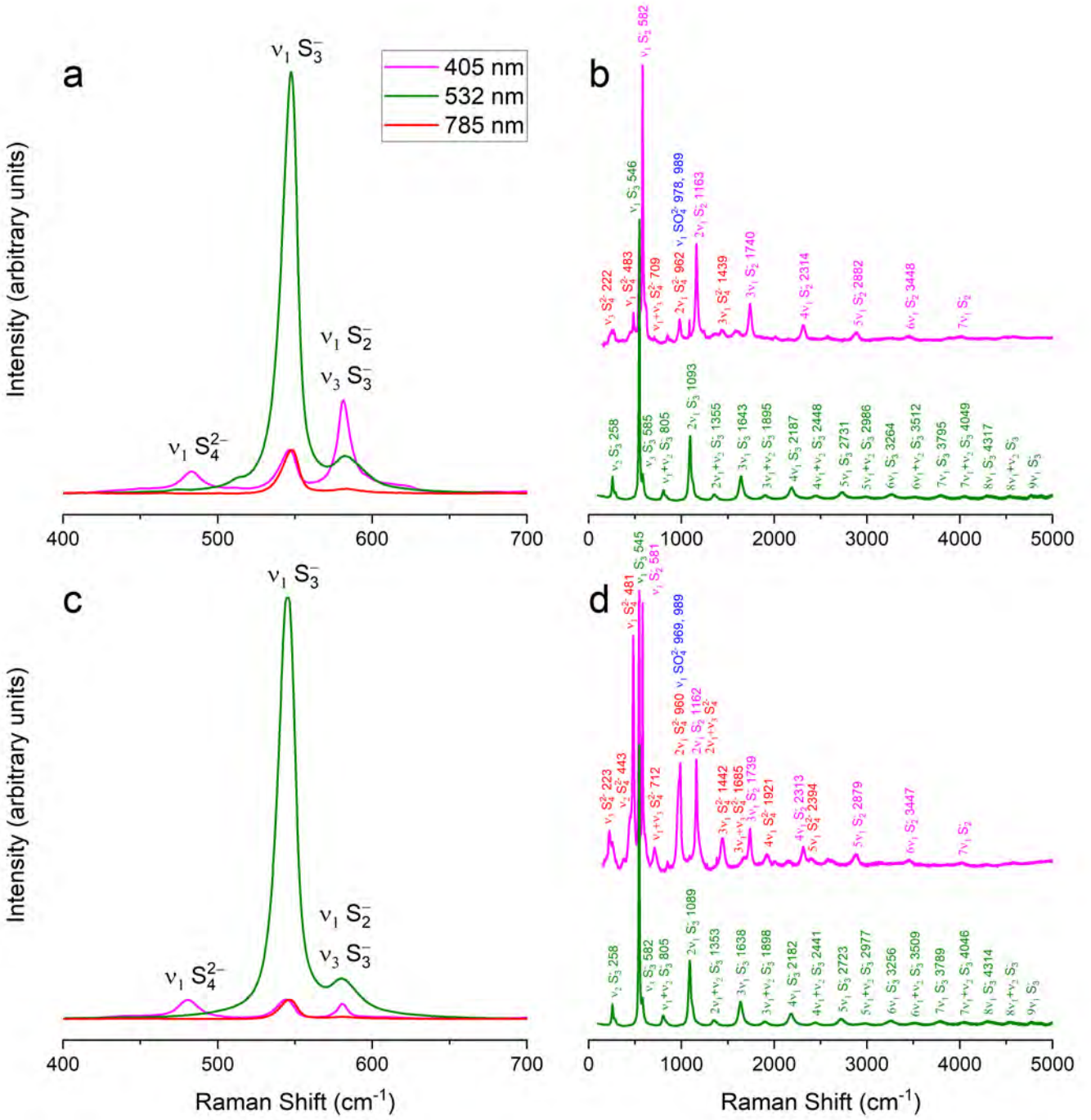
a
b
c
d
405 nm
532 nm
785 nm
Intensity (arbitrary units)
Raman Shift (cm-1)
ν1 S3-
ν1 S2-
ν3 S3-
ν1 S4 2-
ν1 S2 582
ν1 S3 546
ν1 S4 2- 483
ν1 S4 2- 222
ν1+ν3 S4 2- 709
ν1 SO4 2- 978, 989
2ν1 S4 2- 962
2ν1 S2 1163
3ν1 S4 2- 1439
3ν1 S2 1740
4ν1 S2 2314
5ν1 S2 2882
6ν1 S2 3448
7ν1 S2
ν2 S3 258
ν3 S3 585
ν1+ν2 S3 805
2ν1 S3 1093
2ν1+ν2 S3 1355
3ν1 S3 1643
3ν1+ν2 S3 1895
4ν1 S3 2187
4ν1+ν2 S3 2448
5ν1 S3 2731
5ν1+ν2 S3 2986
6ν1 S3 3264
6ν1+ν2 S3 3512
7ν1 S3 3795
7ν1+ν2 S3 4049
8ν1 S3 4317
8ν1+ν2 S3
9ν1 S3
ν1 S3 581
ν1 S4 2- 481
ν1 S4 2- 223
ν2 S4 2- 443
ν1+ν3 S4 2- 712
2ν1 S4 2- 960
2ν1 S2 1162
2ν1+ν3 S4 2-
3ν1 S4 2- 1442
3ν1+ν3 S4 2- 1685
3ν1 S2 1739
4ν1 S4 2- 1921
4ν1 S2 2313
5ν1 S4 2- 2394
5ν1 S2 2879
6ν1 S2 3447
7ν1 S2
2ν1 S3 1089
2ν1+ν2 S3 1353
3ν1 S3 1638
3ν1+ν2 S3 1898
4ν1 S3 2182
4ν1+ν2 S3 2441
5ν1 S3 2723
5ν1+ν2 S3 2977
6ν1 S3 3256
6ν1+ν2 S3 3509
7ν1 S3 3789
7ν1+ν2 S3 4046
8ν1 S3 4314
8ν1+ν2 S3
9ν1 S3

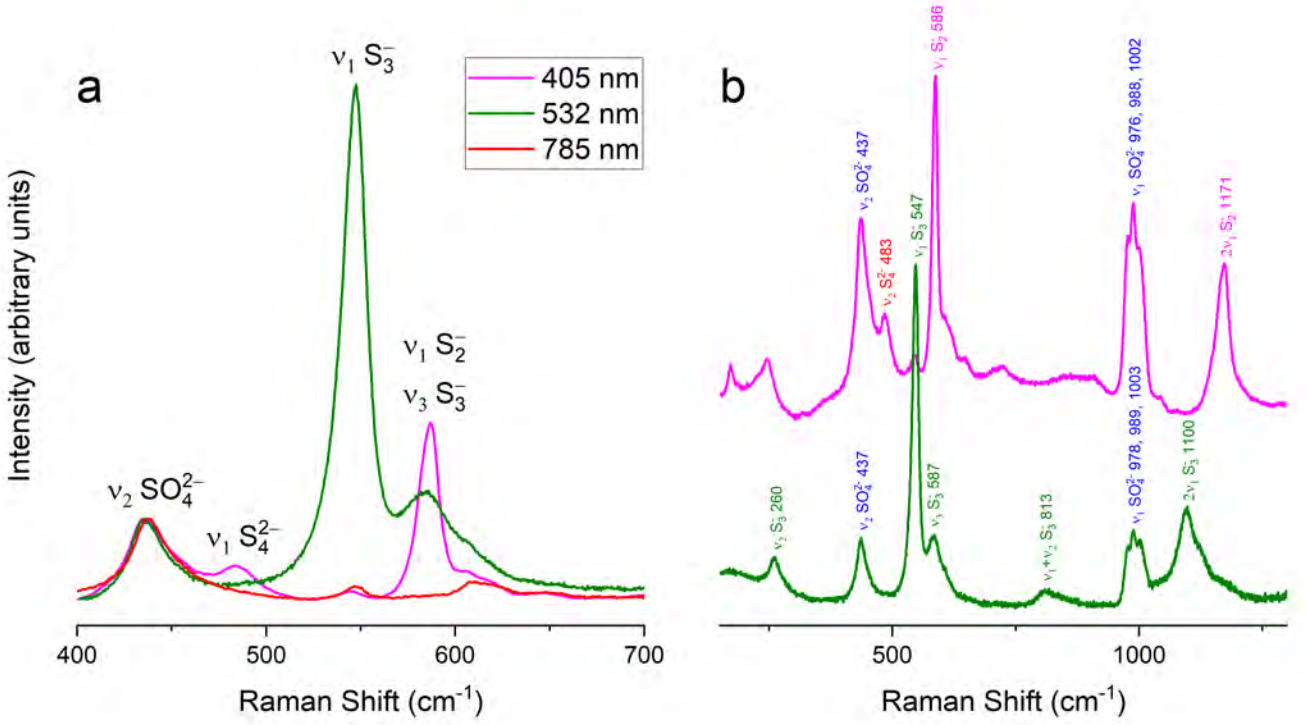
a
405 nm
532 nm
785 nm
Intensity (arbitrary units)
ν1 S3−
ν1 S2−
ν3 S3−
ν2 SO4 2−
ν1 S4 2−
400
500
600
700
Raman Shift (cm-1)
b
ν2 SO4 2- 437
ν2 S4 2- 483
ν1 S3- 547
ν1 S2- 586
ν1 SO4 2- 976, 988, 1002
2ν1 S2- 1171
ν2 S3- 260
ν2 SO4 2- 437
ν3 S3- 587
ν1+ν2 S3 813
ν1 SO4 2- 978, 989, 1003
2ν1 S3 1100
500
1000
Raman Shift (cm-1)

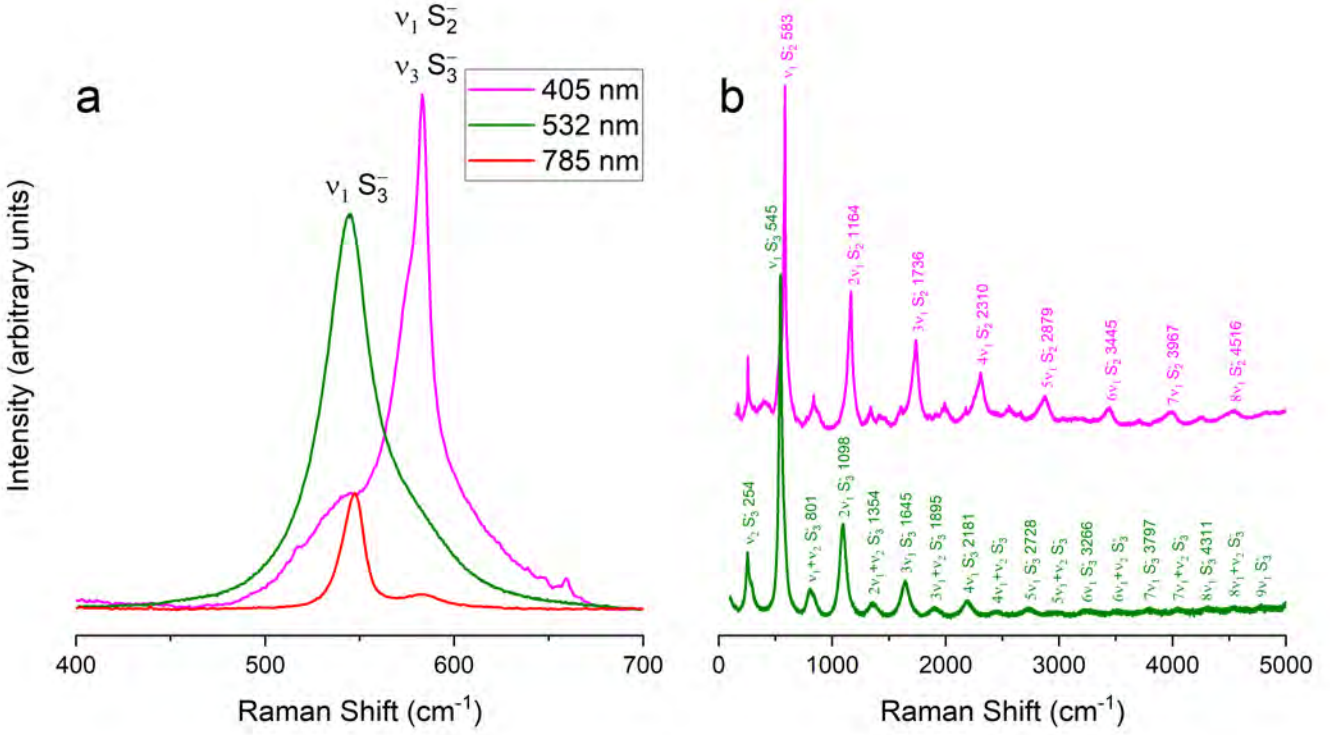
a
b
ν_1 S_2^-
ν_3 S_3^-
ν_1 S_3^-
405 nm
532 nm
785 nm
Intensity (arbitrary units)
Raman Shift (cm^{-1})
400
500
600
700
0
1000
2000
3000
4000
5000
ν_1 S_2^- 583
ν_1 S_3^- 545
$2\nu_1$ S_2^- 1164
$3\nu_1$ S_2^- 1736
$4\nu_1$ S_2^- 2310
$5\nu_1$ S_2^- 2879
$6\nu_1$ S_2^- 3445
$7\nu_1$ S_2^- 3967
$8\nu_1$ S_2^- 4516
ν_2 S_3^- 254
$\nu_1+\nu_2$ S_3^- 801
$2\nu_1$ S_3^- 1098
$2\nu_1+\nu_2$ S_3^- 1354
$3\nu_1$ S_3^- 1645
$3\nu_1+\nu_2$ S_3^- 1895
$4\nu_1$ S_3^- 2181
$4\nu_1+\nu_2$ S_3^-
$5\nu_1$ S_3^- 2728
$5\nu_1+\nu_2$ S_3^-
$6\nu_1$ S_3^- 3266
$6\nu_1+\nu_2$ S_3^-
$7\nu_1$ S_3^- 3797
$7\nu_1+\nu_2$ S_3^-
$8\nu_1$ S_3^- 4311
$8\nu_1+\nu_2$ S_3^-
$9\nu_1$ S_3^-

Figure 5

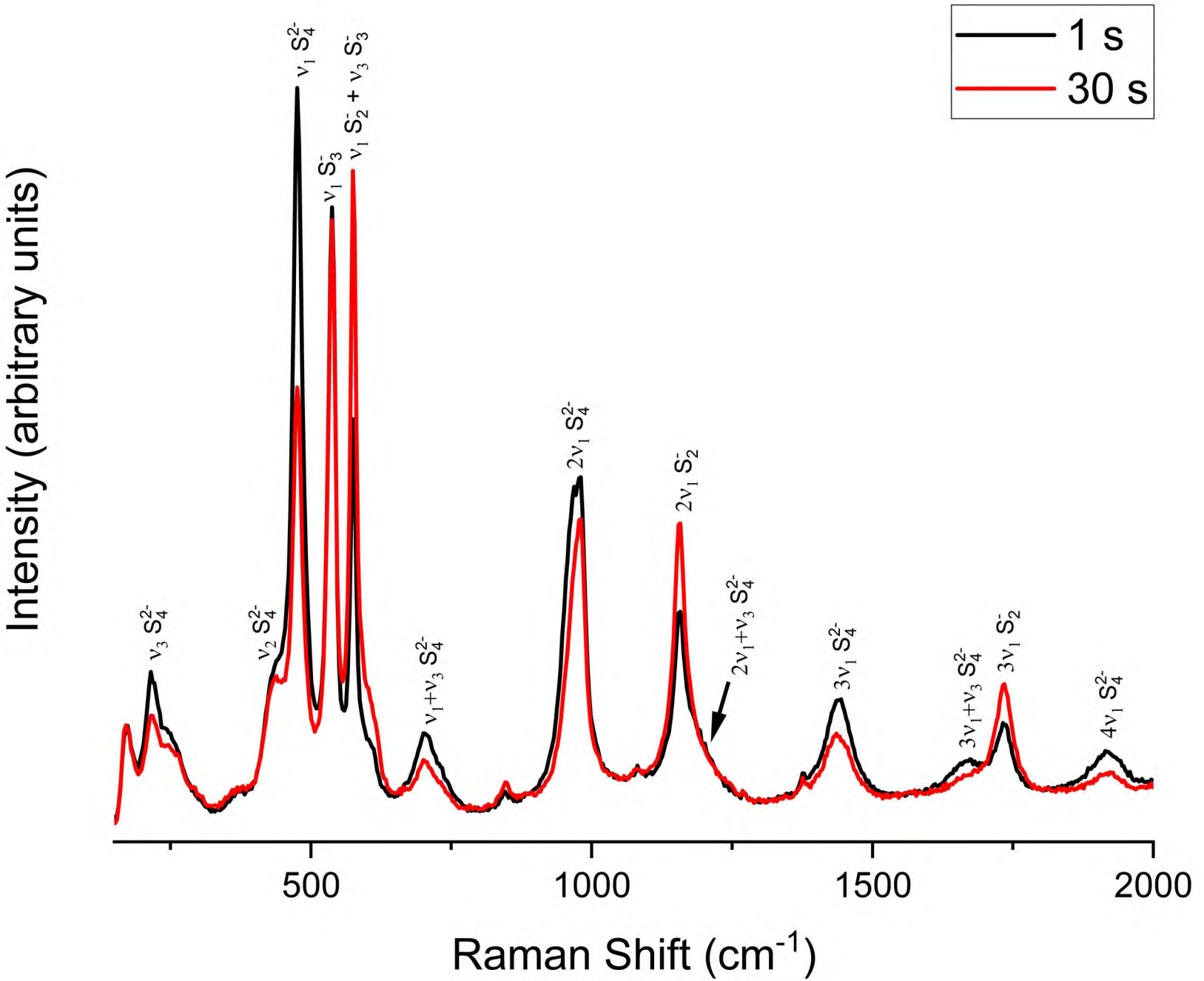
1 s
30 s
Intensity (arbitrary units)
Raman Shift (cm-1)
500
1000
1500
2000
ν3 S4 2-
ν2 S4 2-
ν1 S4 2-
ν1 S3 -
ν1 S2 - + ν3 S3 -
ν1+ν3 S4 2-
2ν1 S4 2-
2ν1 S2 -
2ν1+ν3 S4 2-
3ν1 S4 2-
3ν1+ν3 S4 2-
3ν1 S2 -
4ν1 S4 2-

Figure 6

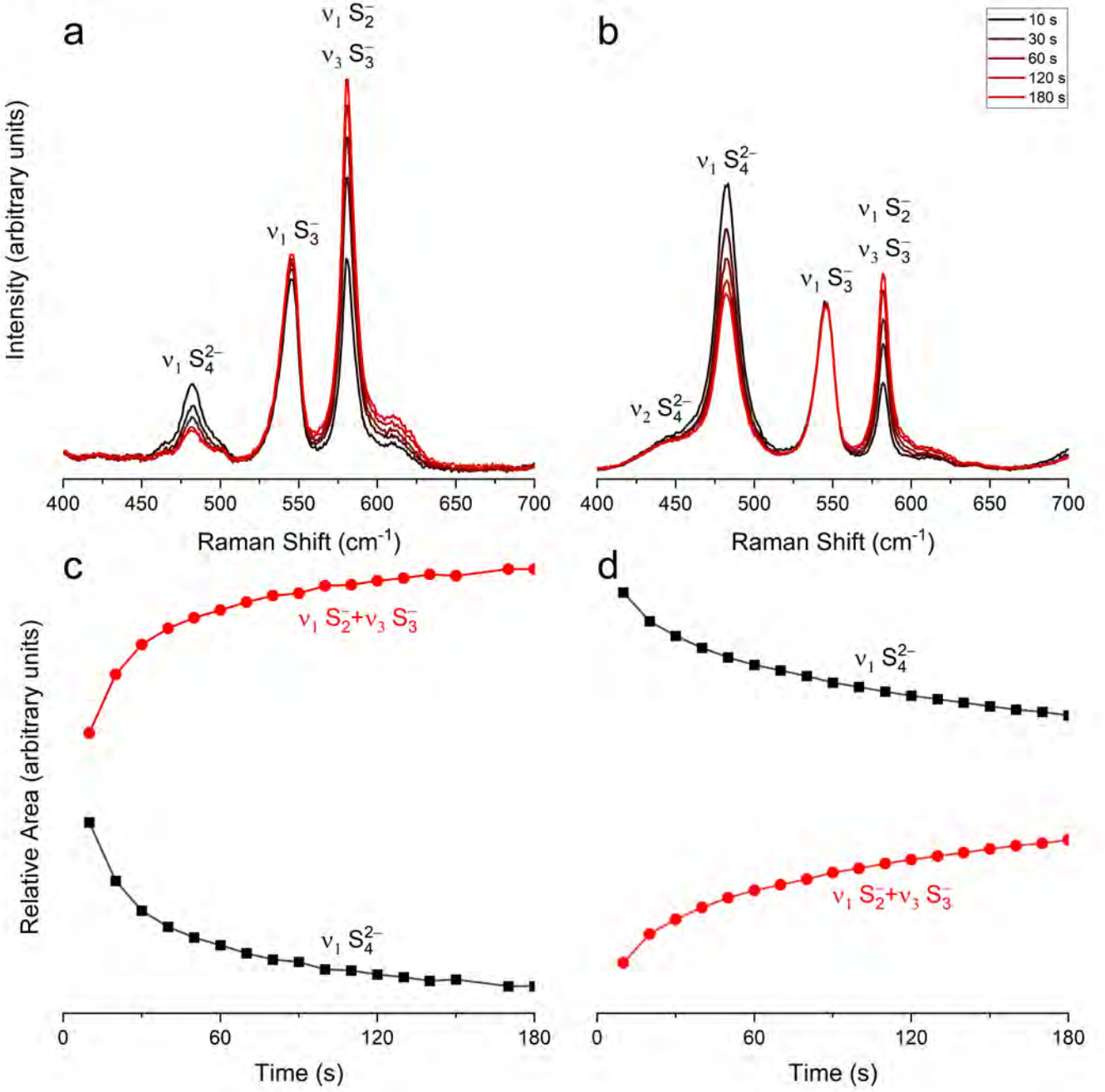
a
b
c
d
10 s
30 s
60 s
120 s
180 s
Intensity (arbitrary units)
Raman Shift (cm-1)
Relative Area (arbitrary units)
Time (s)
ν1 S2−
ν3 S3−
ν1 S3−
ν1 S4 2−
ν2 S4 2−
ν1 S2−+ν3 S3−
400
450
500
550
600
650
700
0
60
120
180

Figure 7

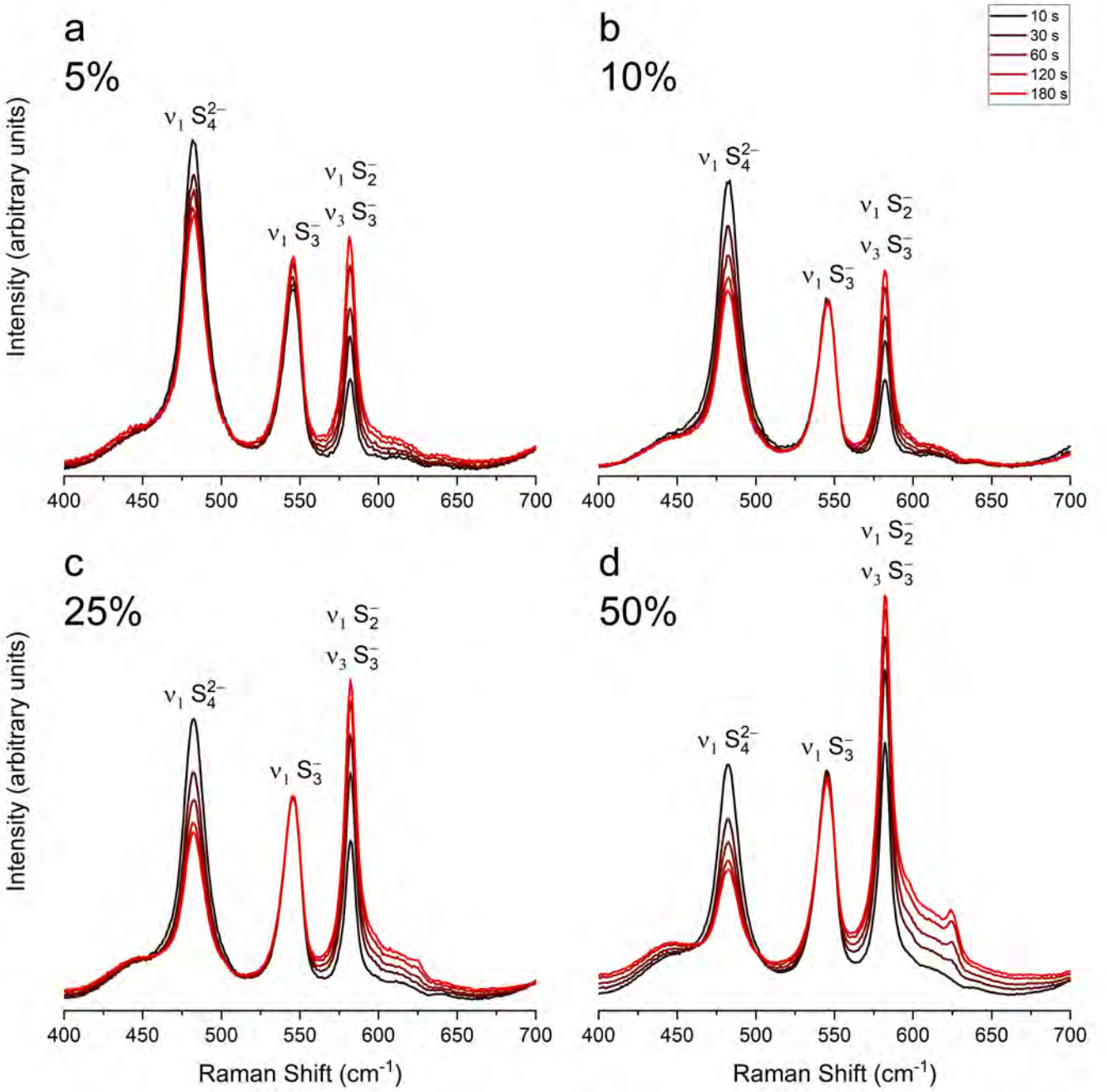
a
5%
b
10%
c
25%
d
50%
10 s
30 s
60 s
120 s
180 s
Intensity (arbitrary units)
Raman Shift (cm-1)
ν1 S4 2−
ν1 S3 −
ν1 S2 −
ν3 S3 −
400
450
500
550
600
650
700

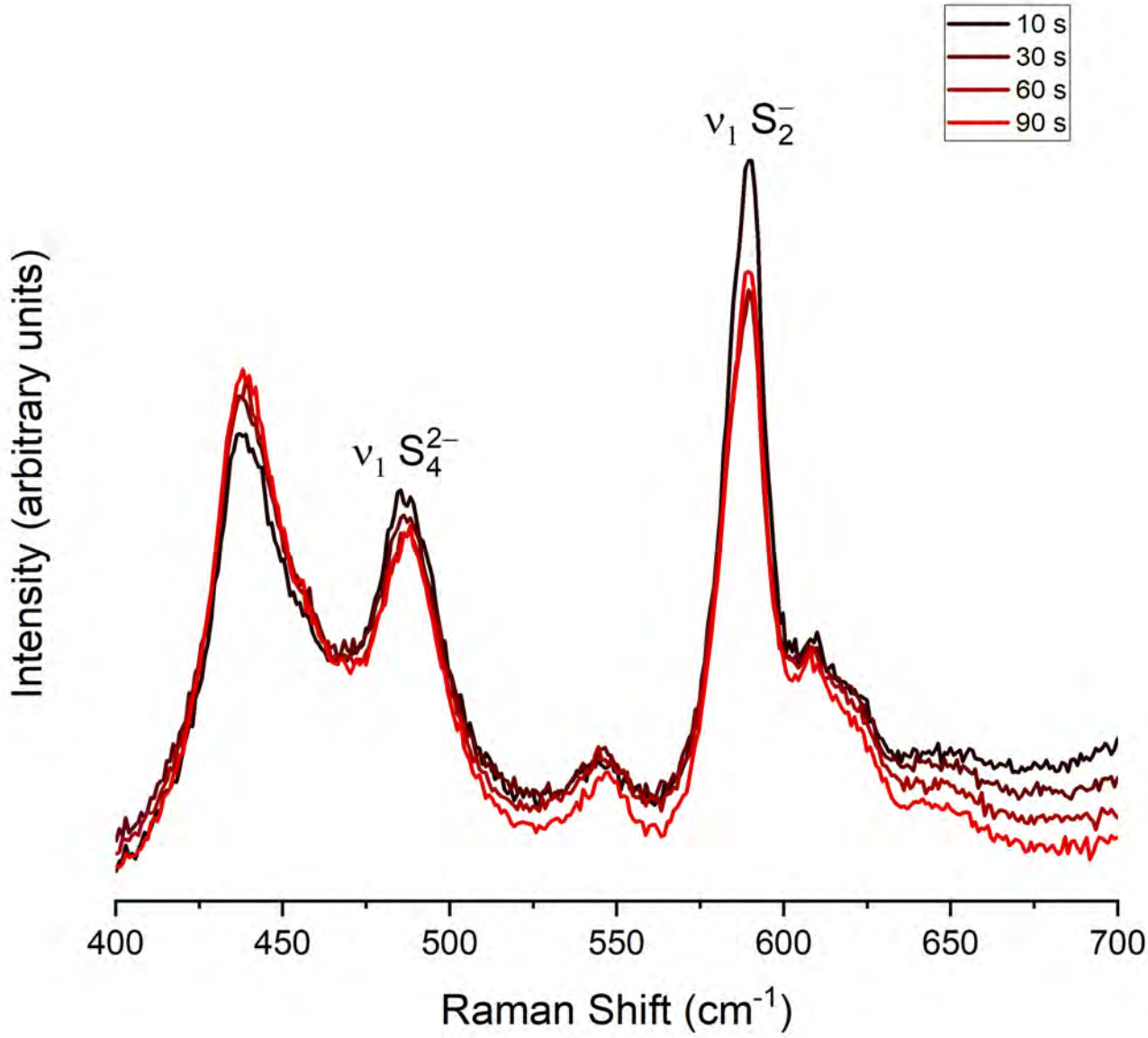
10 s
30 s
60 s
90 s
ν_1 S_2^-
ν_1 S_4^{2-}
Intensity (arbitrary units)
400
450
500
550
600
650
700
Raman Shift (cm^{-1})

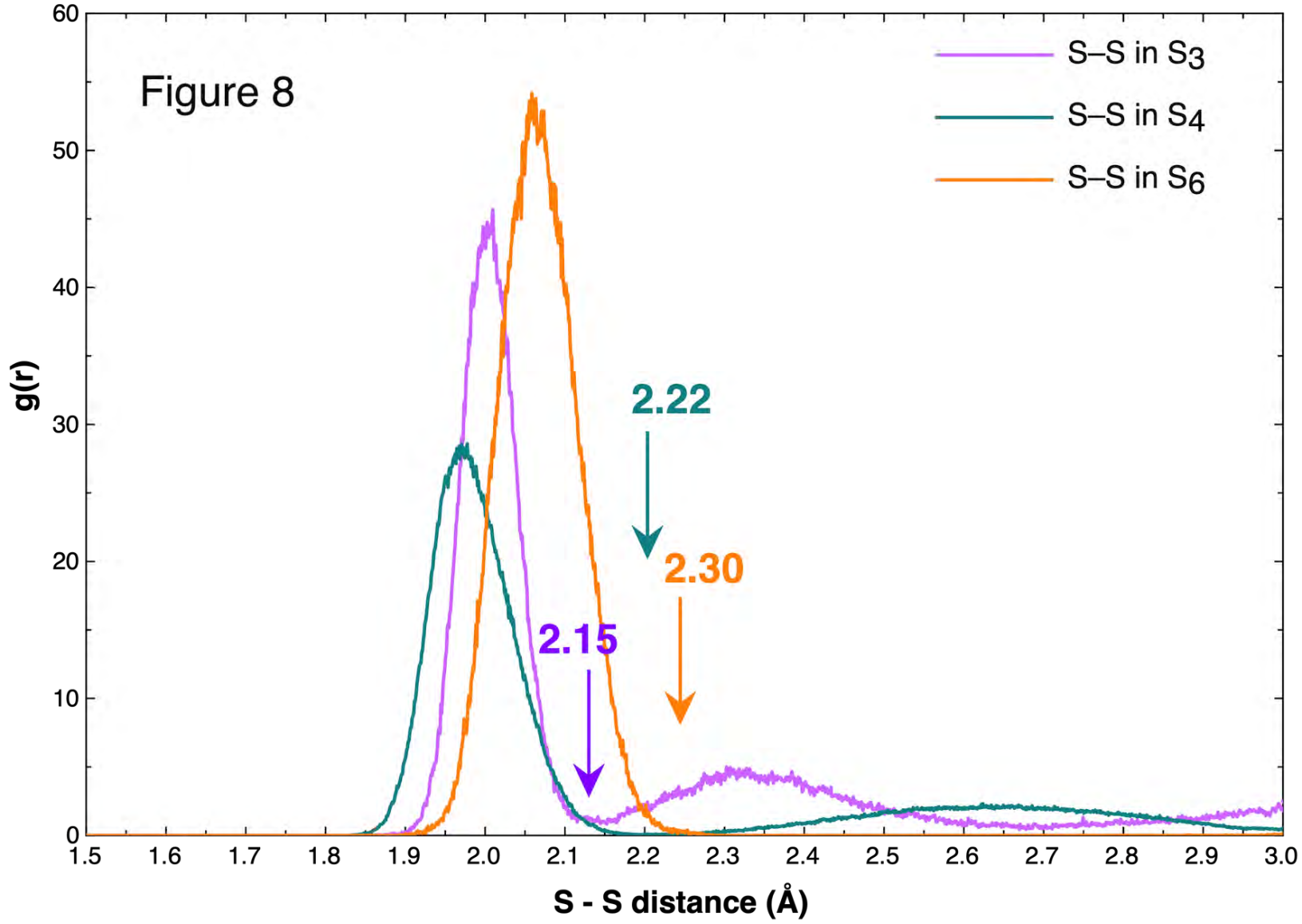
Figure 8
S–S in S3
S–S in S4
S–S in S6
2.22
2.30
2.15
g(r)
S - S distance (Å)
0
10
20
30
40
50
60
1.5
1.6
1.7
1.8
1.9
2.0
2.1
2.2
2.3
2.4
2.5
2.6
2.7
2.8
2.9
3.0